J. Ocean Univ. China (Oceanic and Coastal Sea Research)
https://doi.org/10.1007/s11802-021-4611-9
ISSN 1672-5182, 2021 20 (2): 349-360
http://www.ouc.edu.cn/xbywb/
E-mail:xbywb@ouc.edu.cn

Facile Synthesis of Fe/Cr-Codoped ZnO Nanoparticles with Excellent Adsorption Performance for Various Pollutants

SUN Yongkai[1)], LUO Siqi[1)], XING Jing[2)], LI Zhenjiang[1), *], and MENG Alan[3), *]

1) *College of Electromechanical Engineering*, *Qingdao University of Science and Technology*, *Qingdao* 266061, *China*
2) *Gaomi Campus*, *Qingdao University of Science and Technology*, *Gaomi* 266000, *China*
3) *Key Laboratory of Sensor Analysis of Tumor Marker*, *Ministry of Education*, *College of Chemistry and Molecular Engineering*, *Qingdao University of Science and Technology*, *Qingdao* 266042, *China*

(Received May 29, 2020; revised October 20, 2020; accepted October 29, 2020)

Abstract Adsorption is an effective and low-cost method for removing antibiotics and dyes. However, it remains a challenge to prepare an adsorbent with excellent adsorption properties for both various antibiotics and dyes. Herein, Fe/Cr-codoped ZnO with high adsorption capacity and fast adsorption rate are prepared by an environmentally friendly solvothermal method. Fe/Cr-codope ZnO with a diameter of 10–20 nm exhibits superior adsorption capacities for the antibiotics of tetracycline hydrochloride (TC-HCl) (826.45 mg g^{-1}) and tetracycline (TC) (331.01 mg g^{-1}), and anionic dyes of methyl orange (MO) (1023.88 mg g^{-1}), methyl blue (MB) (726.26 mg g^{-1}) and direct red (DR) (642.25 mg g^{-1}). Meanwhile, it presents fast adsorption rate, it only took 30 min to reach more than 90% of the equilibrium adsorption amount for TC-HCl, TC, MO, MB and DR. The adsorption process closely fitted the Langmuir isotherm model and pseudo second-order rate equation. More importantly, simple method has been developed for separating the pollutant from the adsorbent, which not only regenerates the materials, but also completes the recovery of antibiotics and dyes, avoiding the secondary pollution. The broad-spectrum, rapid, environment-friendly and effective adsorption properties make Fe/Cr-codoped ZnO a promising adsorbent for water treatments.

Key words antibiotics; dyes; codoped; adsorption; regeneration

1 Introduction

In recent years, antibiotics are widely used in the treatment of many diseases as well as the production of animal feed. Coincidentally, dyes are also widely applied to many industrial fields (Yao *et al*., 2016; Shen *et al*., 2018; Zou *et al*., 2020). In the past decades, with the widespread utilization and rapid depletion of antibiotics and dyes, a large amount of them have been discharged into the environmental system in the form of waste water or feces. Antibiotics (Zhou *et al*., 2013; Zhu *et al*., 2013; Li *et al*., 2020) and dyes entering the environmental system can bring serious threats to the survival of plants and animals even to human health (Das *et al*., 2013; Okesola *et al*., 2016; Hu *et al*., 2018) and will cause water pollution problems on a massive scale. Therefore, the severe environment pollution and the terrible health threats from antibiotics and dyes effluent will further aggravate the urgent need of developing a highly efficient, environmentally friendly, and cost-effective novel functional material for wastewater treatment.

* Corresponding authors. E-mail: zhenjiangli@qust.edu.cn
E-mail: alanmengqust@163.com

Accordingly, various wastewater treatment technologies techniques have been proposed, such as adsorption, biodegradation, ion exchange, membrane separation, coagulation and photocatalysis, *etc* (Li *et al*., 2013; Ge *et al*., 2016; Huang *et al*., 2017; Lo *et al*., 2017; Li *et al*., 2018; Qi *et al*., 2018). However, due to the wide range and refractory properties of antibiotics and dyes, most of the water treatment methods are not ideal for the wastewater containing antibiotics and dyes. And it is noteworthy that adsorption has been proven to be a well-established and economical approach for the wastewater treatment thanks to its low cost, short equilibrium time and simple operation (Ge *et al*., 2016; Chen *et al*., 2018; Huang *et al*., 2018).

The key problem for the application of the adsorption method is to synthesize adsorbent with high adsorption property (Peng *et al*., 2014; Chen *et al*., 2016; Zhang *et al*., 2018). Different types of adsorbents are developed to remove pollutants from wastewater, such as carbon materials (Perreault *et al*., 2015; Musielak *et al*., 2019), porous materials (Wu *et al*., 2012; Yang *et al*., 2014; Wang *et al*., 2015), biomaterials, polymers materials (Roosen *et al*., 2014; Zheng *et al*., 2014; Rekha *et al*., 2016; Zhao *et al*., 2017). However, practically, those methods are still unable to meet the demand due to their low adsorption ca-

pacity, long adsorption time, or second pollution. It is necessary to carry out further research and develop advanced adsorbents with high adsorption capacity and a rapid adsorption rate for antibiotics and organic dyes. Inorganic non-metallic materials have good oxidation resistance, wear resistance and corrosion resistance. They have been attracted widely attention of researchers and are often used as adsorption materials. Although the inorganic nonmetallic material adsorbent has good development prospects, the silica powder is toxic and has potential damage to the human health. Additionally, the preparation technology of carbon-based inorganic nonmetallic adsorbent is complex and low yield, so it cannot be widely used in wastewater treatment. Zinc oxide has been widely used in many fields such as light, electricity and catalysis (Izaki *et al*., 2013; Zhang *et al*., 2014; Hsu *et al*., 2017) because of its low cost, stable property and environmental friendliness, but rarely apply to the field of water treatment due to its low adsorption capacity and long equilibrium times. Recently, the pure zinc oxide were modified to overcome its inherent defects, such as doping, (Li *et al*., 2008; Song *et al*., 2011) making it has practical application value in the field of adsorption. For example, Xiangning Zheng and his colleagues synthesized the magnetic ZnO clay nanocomposite hydrogel with good adsorption property for La (III) (58.8 mg g^{-1}) (Zheng *et al*., 2014; Perreault *et al*., 2015). Despite of the good achievement they have made, it is still meaningful for obtaining ZnO modified by co-doping two metal ions to acquire the excellent adsorption performance, especially, it could adsorb on the various the antibiotics and dyes meanwhile. In addition, the selection of doped elements should meet the following two requirements. First of all, the doped elements can make the adsorbent surface with more positive charge; in the second place, the doped elements should have ionic radius close to that of zinc. Based on the above considerations, we then choose Fe and Cr with higher valence state as the doped elements in this work.

Herein, a mild one-step-solvothermal method was exploited to prepare Fe/Cr-codoped ZnO NPs with splendid adsorption capacity for the various antibiotisc and dyes. Meanwhile, a range of experiments were executed to investigate various factors affecting the adsorbability of adsorbent, such as pH of solution, initial concentration and contact time. Kinetics and isotherms model manifested that the as-prepared sample takes on the fast adsorption rate as well as high adsorption capacity of 826.45 mg g^{-1} for tetracycline hydrochloride (TC-HCl), 331.01 mg g^{-1} for tetracycline (TC), 1023.88 mg g^{-1} for methyl orange (MO), 726.26 mg g^{-1} for methyl blue (MB) and 642.25 mg g^{-1} for direct red (DR), respectively. The proposed adsorption mechanism reasonably explains the effective removal of the various antibiotics and anion pollutants by Fe/Cr-codoped ZnO NPs. What's more, the regeneration channel of the adsorbent was acquired, making the pollutant and adsorbent can be separated simply and efficiently.

2 Materials and Methods

2.1 Chemicals and Instruments

The $Zn(NO_3)_2{\cdot}6H_2O$, $Cr(NO_3)_3{\cdot}9H_2O$, $Fe(NO_3)_3{\cdot}9H_2O$, NaOH and ethanol absolute were all purchased from Sinopharm Chemical Reagent Co., Ltd., (China). All the chemicals are analytical grade and without further treatment.

Absorbance spectra of pollutants were measured using a UV-vis spectrophotometer (Perkin Elemr, Lambda 35, USA). The morphology of the as-prepared products was acquired using scanning electron microscope (SEM, JSM-6460LV) and transmission electron microscope (TEM, JEM-2100). Crystalline structure of adsorbents was characterized using X-ray diffraction (XRD, D/MAX-2500/PC, CuKa). X-ray Photoelectron Spectroscopy (XPS) pattern was conducted on Thermoelectron spectroscopy (ESCALAB 250, Al Ka = 1486.6 eV, approximately 5×10^{-9} torr).

2.2 Synthesis of Fe/Cr-Codoped ZnO NPs

Firstly, the Fe/Cr-codoped ZnO NP was synthesized by a solvothermal method in a Teflon-lined stainless autoclave. Specifically, 2.0 mmol of $Zn(NO_3)_2{\cdot}6H_2O$, 0.5950 g $Cr(NO_3)_3{\cdot}9H_2O$ and a certain amount of $Fe(NO_3)_3{\cdot}6H_2O$ were absolutely dissolved in 40 mL ethanol absolute at room temperature, and the solution was stirred for 30 min. Then, 4.0 mol L^{-1} NaOH solution (40 mL) was dropped into the above solution. After stirring for 1 h at room temperature, the mixture was transferred into autoclave, heated 12 h at 120℃ in an oven. After natural cooled to room temperature, the products were centrifuged, washed, and freeze-dried for 8 h.

2.3 Adsorption Experiments

Adsorption experiments of typically antibiotics and dyes wastewater (TC-HCl, TC, MO, MB and DR) were carried out in batch adsorption experiments at room temperature (25℃). In the single wastewater system, 10 mg of Fe/Cr-codoped ZnO was added into 30 mL of solution containing antibiotics (TC-HCl and TC) or dyes (MO, MB and DR) with different initial concentrations (the initial concentrations of TC-HCl, MO, MB and DR is 100, 200, 300, 400, 600, 800 and 1000 mg L^{-1}, respectively, and the initial concentrations of TC is 50, 75, 100, 150, 200, 250, 300 mg L^{-1}) at room temperature, and the pH values of the initial solution were adjusted from 6.0 to 11.0 using 0.1 mol L^{-1} HCl and 0.1 mol L^{-1} NaOH solution. In the adsorbing process, 3 mL of wastewater sample was taken out at definite time up to 12 h and then centrifuge. Concentration of the remaining contaminant solution was determined using a UV-vis spectrophotometer.

The adsorption capacities at any time q_t (mg g^{-1}), and the adsorption capacities at equilibrium q_e (mg g^{-1}) of the contaminant on Fe/Cr-codoped ZnO NPs can be calculated using the following Eqs. (1)–(2).

$$q_t = \frac{C_0 - C_t}{m} \times V, \quad (1)$$

$$q_e = \frac{C_0 - C_e}{m} \times V, \quad (2)$$

where C_0 and C_e are the initial and equilibrium concentrations of contaminant in the solution (mg L^{-1}), respectively, q_e is the quantity of adsorbed contaminant on Fe/Cr-codoped ZnO NPs adsorbent at equilibrium (mg g^{-1}), V is the volume of the contaminant solution (L), and m is the mass of Fe/Cr-codoped ZnO NPs sample (g). All the adsorption tests were carried out in triplicates, and the data in this paper were the average measurements.

2.4 Regeneration of Fe/Cr-Codoped ZnO NPs

Firstly, 20 mL 1 mol L^{-1} HNO_3 was added into a beaker containing 0.8 g of Fe/Cr-codoped ZnO NPs absorbed contaminant drop by drop until the particles were completely dissolved; secondly, 1 mol L^{-1} NaOH was added into the above solution until the pH is 8, forming a hydroxide flocculent precipitate; thirdly, the precipitate was obtained by centrifugation; fourthly, the precipitate obtained by centrifugation was washed multiple times, and then dried at 60℃ for 8 h; finally, it was calcined at 180℃ for 2 h.

3 Results and Discussion

3.1 Material Characterization

XRD measurements were performed to investigate the crystal structure of the samples. XRD pattern of ZnO and Fe/Cr-codoped ZnO in Fig.1 showed similar pattern, and several peaks corresponding crystal plane of (100), (002), (101), (102), (110), (103), (200), (112), (201), respectively, which is consistent with wurtzite-phase ZnO crystal (JCPDS No. 36-1451) (Li *et al.*, 2018). Moreover, there was no other peaks appeared in XRD pattern of Fe/Cr-codoped ZnO NPs, indicating that no second phase products were produced after Fe and Cr were doped in ZnO. In addition, it can be seen from the inset of Fig.1 that the peaks of the doped sample deviates slightly to a large angle, suggesting that the doped elements of the small size enter into the zinc oxide lattice to replace some zinc.

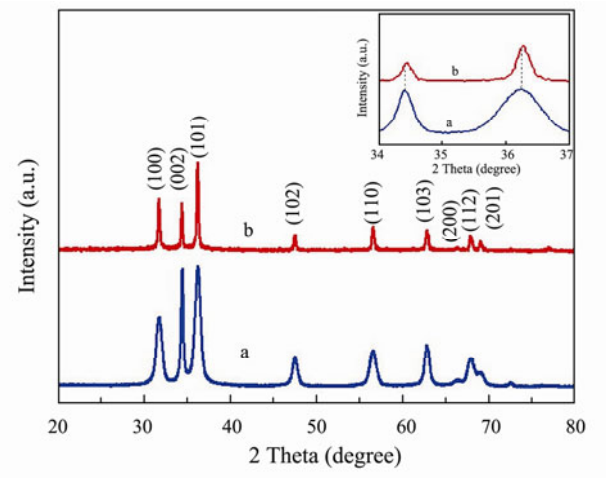

Fig.1 XRD patterns of ZnO (a), Fe/Cr-codoped ZnO (b) NPs and the shift of corresponding diffraction peaks of ZnO and Fe/Cr-codoped ZnO NPs (the inset).

The morphologies of Fe/Cr-codoped ZnO nanoparticles were investigated through SEM and TEM (Fig.2). As can be seen from SEM images (Figs.2A and B), the as-prepared Fe/Cr-codoped ZnO is nanoparticle with a relatively uniform size, whose diameter is approximately 10–20 nm. Fig.2C shows TEM image, indicating that Fe/Cr-codoped ZnO has a homogenous particle size with good dispersion. As shown in Fig.2D, the size of the particles is between 10–20 nm. The inset of Fig.2D shows HRTEM (Chen *et al.*, 2000) pattern of the Fe/Cr-codoped ZnO, and the lattice stripes of the nanoparticles are clear-

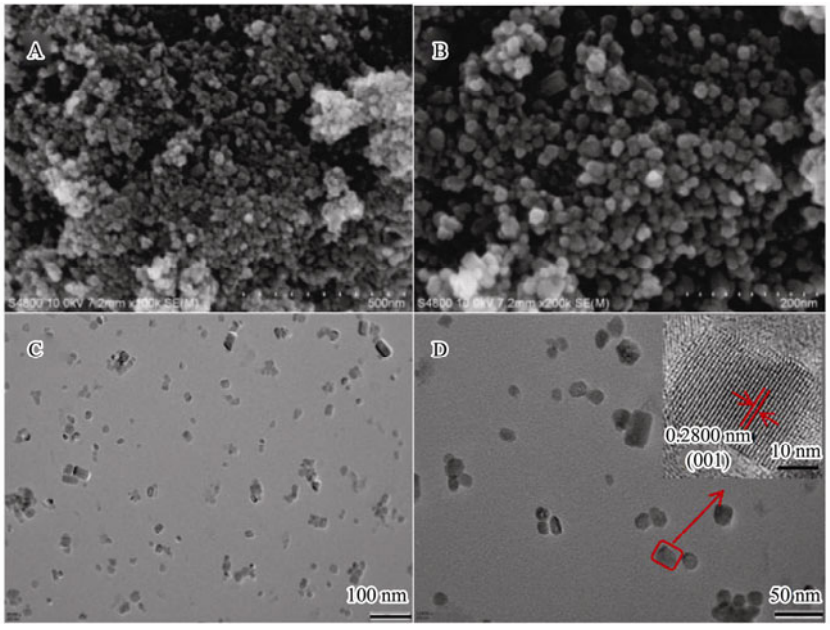

Fig.2 Typical SEM (A, B), TEM (C, D) images of Fe/Cr-codoped ZnO NPs.

ly visible, indicating that the as-prepared sample has good crystallinity, and the spacing of 0.2800 nm correspond to the (100) planes of wurtzite-phase ZnO crystals, which was consistent with the result of XRD.

To furtherly investigate the chemical composition and valence state of the composites, X-ray photoelectron spectroscopy (XPS) analysis of Fe/Cr-codoped ZnO nanoparticles was carried out. The XPS survey spectrum (Fig.3A) clearly indicates that there are peaks of Cr, Fe, Zn, and O elements in Fe/Cr-codoped ZnO. Figs.3B–D shows the high-resolution XPS spectrum of Cr 2p, Fe 2p, and Zn 2p regions, respectively. In Fig.3B, two peaks with binding energies of 577.2 and 586.4 eV are assigned to Cr $2p_{3/2}$ and Cr $2p_{1/2}$, respectively, which correspond to Cr^{3+}. In Fig.3C, the high-resolution Fe 2p spectra show two broad peaks of Fe $2p_{1/2}$ and Fe $2p_{3/2}$ with binding energies of 725.3 and 711.5 eV, respectively, corresponding to Fe^{3+}. The peak at 717.4 eV is attributed to the shakeup satellite peak (denoted as 'Sat.') of Fe^{3+} (Grosvenor *et al*., 2004). The results of XPS can further indicated that Cr^{3+} and Fe^{3+} entered into the lattices of ZnO and substituted the positions Zn^{2+}, which are in accordance with the result of XRD. Peaks at 1022.0 and 1045.1 eV, as shown in Fig. 3D, corresponding to Zn $2p_{3/2}$ and Zn $2p_{3/2}$, respectively, can be assigned to the Zn^{2+} species in the ZnO nanomaterial (Song *et al*., 2016).

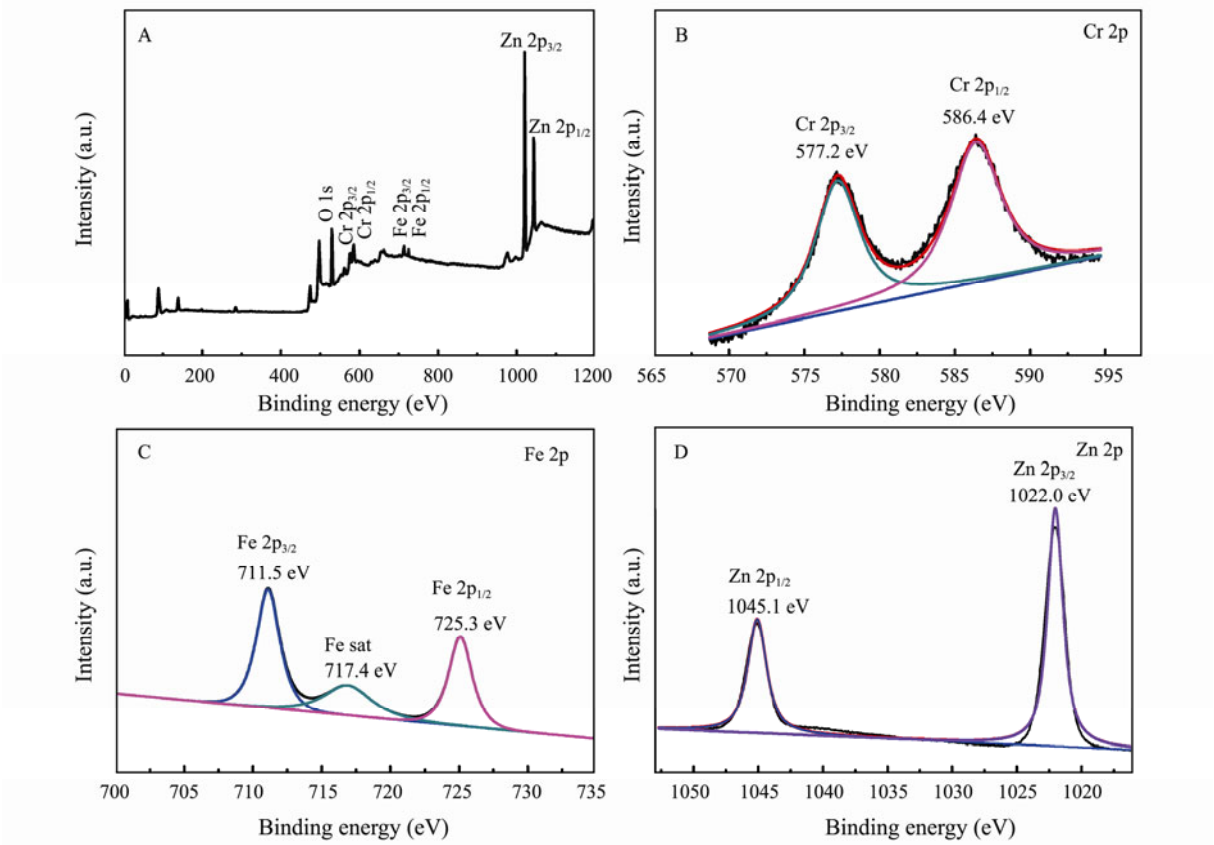

Fig.3 XPS spectra of the Fe/Cr-codoped ZnO NPs. XPS survey spectrum (A); High-resolution XPS spectra of Cr 2p (B); Fe 2p (C) and Zn 2p (D).

3.2 The Effect of Adsorption Conditions on Adsorption Property

To achieve optimistic performance, the effect of adsorption conditions, such as pH values of solution, the initial concentration of pollutants and contact time, on adsorption property were systematically examined.

3.2.1 The effect of pH

The pH of the solution is an important parameter influencing the adsorption capacity of adsorbents. Hence, the effect of pH on the adsorption capacity of pollutants (TC-HCl, TC, MO, MB and DR) over Fe/Cr-codoped ZnO are shown in Fig.4. Fig.4(A) displays the adsorption capacity of Fe/Cr-codoped ZnO under different pH conditions. It can be observed that the adsorption capacity of Fe/Cr-codoped ZnO is increased first and then decreased with the pH value changing in the range of 6–11, reaching the maximum value at pH = 7. The characterization results in Fig.4(B) explain the reasons for this phenomenon. The effect of pH on adsorbent performance is carried out by affecting the surface zeta potential of the adsorbent. The zeta potential of Fe/Cr-codoped ZnO is positive in the range of pH 6–11. The surface of the adsorbent has the greatest positive charge when the pH is 7, so the maximum adsorption capacity was reached at under this condition.

3.2.2 The effect of initial concentration

Different initial concentration of the pollutant may have important effects on the adsorption capacity of the adsorbent. Fig.5A shows the effect of the pollutant initial

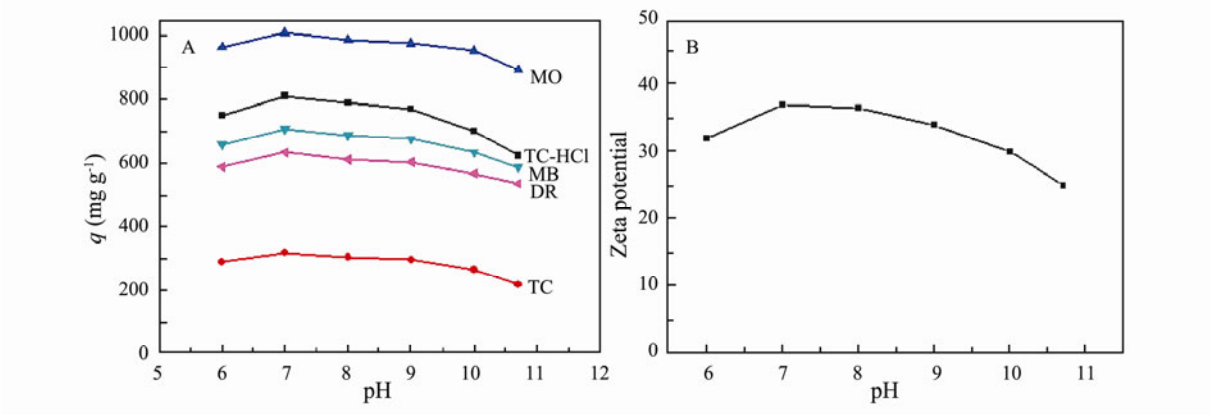

Fig.4 The adsorption capacity (A) and zeta potential (B) of Fe/Cr-codoped ZnO under different pH conditions.

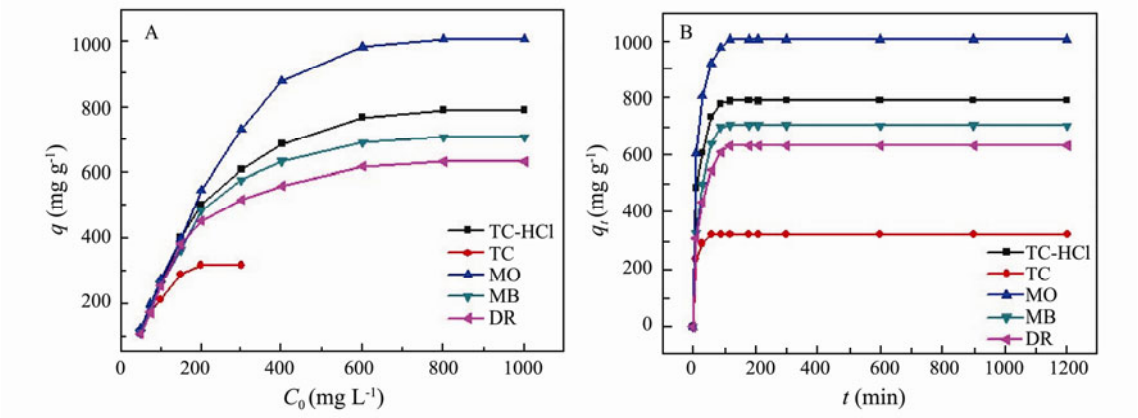

Fig.5 The effect of the initial concentration (A) and contact time profiles (B) of pollutants adsorption on the Fe/Cr-codoped ZnO.

concentration on adsorption capacity of adsorbent. The curve in the Fig.5A shows that the adsorption capacity of adsorbent in equilibrium gradually increases and finally tends to be stable with the pollutant initial concentration increasing. Specifically, when the initial concentration is within the range of 100–400 mg L^{-1} for TC-HCl, MO, MB or DR, the adsorption capacity of adsorbent increases rapidly. While the adsorption capacity changes slowly, when the initial concentration increases within the range of 400–800 mg L^{-1}. Similarly, when the initial concentration is within the range of 50–200 mg L^{-1} for TC, the adsorption capacity of adsorbent increases rapidly. However, when the initial concentration increases within the range of 200–300 mg L^{-1}, the adsorption capacity changes slowly. The reason may be that the increase of the driving force molecules motion with the increase of the pollutant concentration, and then, increasing the chances of collision between pollutant molecules and the active sites on the surface of adsorbent. However, when the initial concentration increases to a certain degree, the available active sites on the adsorbent surface decrease, reducing the rate of collision between the pollutant molecules and the active sites on the surface of the adsorbent, so the adsorption capacity increases slowly. Finally, the adsorbent reaches adsorption saturation. As a result, the concentration of the pollutants continues to increase but the adsorption capacity of adsorbent is no longer increased.

3.2.3 The effect of contact time

Equilibrium time is one of the most important indexes for evaluating the adsorption performance of adsorbent in wastewater treatment systems. In the process of adsorption, the adsorption capacity goes through three stages, from rapid increase to slow increase and finally to equilibrium in Fig.5B. At the first 30 min, the adsorption reaction was rapid proceeding, then the process slowed down, and finally the adsorption equilibrium was reached within 120 min for TC-HCl, MO, MB or DR. Similarly, for TC, during the first 10 min of the reaction, the adsorption increased rapidly, then slowly, and finally reached adsorption equilibrium within 60 min. The explanation for this phenomenon is as follows: at the initial stage of adsorption, a large number of active sites are available on the surface of adsorbent, so adsorbent can quickly absorb pollutant molecules. Later on, as the adsorption progressed, the available active sites on the surface of adsorbent gradually decrease, thus adsorption becomes slow. Finally, all the active sites were occupied, so the adsorbent no longer adsorbed pollutant molecules, and the adsorbent reached adsorption saturation. Fe/Cr-codoped ZnO will have a promising application prospect in waste-water treatment field due to its fast adsorption rate and large adsorption capacity.

3.3 Adsorption Kinetics

Fig.5B indicates the adsorption rate of Fe/Cr-codoped ZnO for TC-HCl, TC, MO, MB and DR are rapid in the initial short time, then gradually slows. To better clarify the adsorption behavior, the adsorption kinetics of Fe/Cr-codoped ZnO are further evaluated by the following adsorption kinetic equations.

Pseudo first-order equation:

$$\ln(q_e - q_t) = \ln q_e - k_1 t, \tag{3}$$

Pseudo second-order equation:

$$\frac{t}{q_t} = \frac{1}{k_2 q_e^2} + \frac{t}{q_e}, \tag{4}$$

wherein q_t and q_e are the adsorption capacity (mg g^{-1}) at time t and the equilibrium, respectively; and k_1 (min^{-1}) and k_2 (g (mg min)$^{-1}$) are the adsorption rate constant.

To analyze the adsorption process of Fe/Cr-codoped ZnO, pseudo-first-order (PFO) and pseudo-second-order (PSO) kinetic models were used to fit the experimental data. The results of the kinetic model simulation were

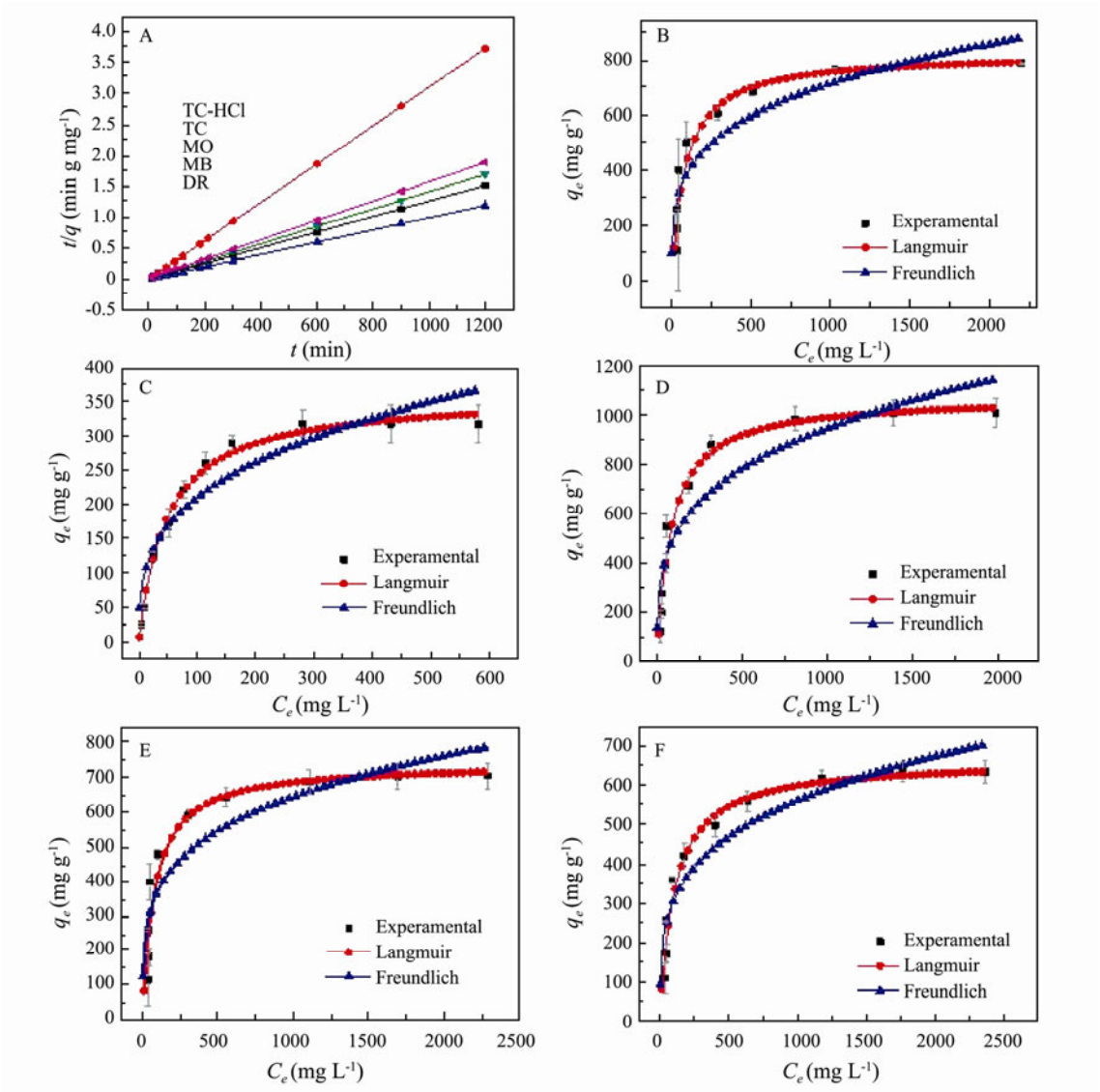

Fig.6 Pseudo-second-order adsorption kinetics of pollutants (A) and adsorption isotherm of TC-HCl (B), TC (C), MO (D), MB (E) and DR (F) on Fe/Cr-codoped ZnO.

Table 1 Adsorption kinetic parameters of pollutants on Fe/Cr-codoped ZnO (25℃, pH=7.0)

Adsorbate	q_e (exp.) (mg g^{-1})	Pseudo-second-order		
		k_2 (g mg^{-1} min^{-1})	q_e (cal)	R^2
TC-HCl	806.37	3.76×10^{-4}	793.65	0.9999
TC	320.56	2.55×10^{-3}	321.54	0.9999
MO	1008.56	2.51×10^{-4}	1013.17	0.9999
MB	706.18	2.86×10^{-4}	709.22	0.9999
DR	632.68	2.73×10^{-4}	636.94	0.9999

Table 2 Adsorption kinetic parameters of pollutants on Fe/Cr-codoped ZnO (25℃, pH=7.0)

Adsorbate	q_e (exp) (mg g^{-1})	Pseudo-first-order		
		k_1 (min^{-1})	q_e (cal)	R^2
TC-HCl	806.37	0.1256	770.25	0.9486
TC	320.56	0.1995	317.98	0.9705
MO	1008.56	0.1113	984.53	0.9645
MB	706.18	0.0645	690.45	0.9380
DR	632.68	0.0734	617.31	0.9263

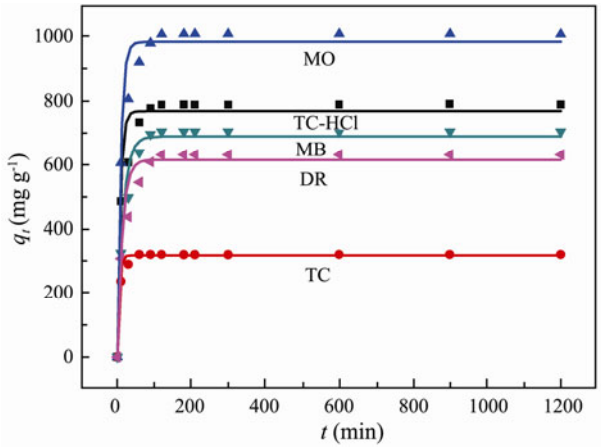

Fig.7 Pseudo-first-order adsorption kinetics of pollutants on Fe/Cr-codoped ZnO.

shown in Fig.6 and Fig.7, and the relative parameters were tabulated in Table 1 and Table 2. In Fig.6(A), the experimental data of the investigated several adsorbents can be well fitted to the pseudo-second-order kinetic model, and R^2 (correlation coefficient) of PSO for five pollutants are all exceeds 0.9999 (Table 1), indicating that chemisorption is the rate-determining step in the adsorption process (Li *et al*., 2019).

3.4 Adsorption Isotherms

To quantitatively analyze the adsorption behaviors and mechanism of Fe/Cr-codoped ZnO adsorbent, the adsorption data of the adsorbent over the pollutants are fitted by Langmuir and Freundlich isotherm models (Fig.6(B–F)). The Langmuir and Freundlich isotherm model equations are

$$\frac{c_e}{q_e}=\frac{c_e}{q_m}+\frac{1}{K_L q_m}, \tag{5}$$

$$q_e = K_F c_e^{\,1/n}, \tag{6}$$

where c_e is the concentration (mg L^{-1}) of the pollutant solution when the adsorption reaches equilibrium; q_e is the equilibrium adsorption capacity (mg g^{-1}); q_m is the maximum adsorption capacity (mg g^{-1}); K_L is the Langmuir isothermal constant (L mg^{-1}); K_F is the Freundlich isothermal constant (mg g^{-1}) (L mg)$^{1/n}$; and n is the factor relating to the adsorption intensity.

The Langmuir isotherm model supposes that adsorption occurs on a uniform surface with homogeneous active sites through monolayer adsorption. Hence, it can reach saturation. Whereas, the Freundlich isotherm adsorption model assumes that multilayer adsorption occurs on heterogeneous surfaces. The isotherms of TC-HCl, TC, MO, MB and DR adsorption onto Fe/Cr-codoped ZnO are shown in Fig.6(B–F), and the relative parameters are listed in Table 3. By comparing the R^2 of five pollutants, it is indicated that Langmuir model has better relativity than Freundlich model. This suggests that the adsorption behavior occurs in the form of monolayer on the heterogeneous surfaces of Fe/Cr-codoped ZnO nanoparticles. Furthermore, the saturated adsorption capacity of Fe/Cr-codoped ZnO for various anionic organic pollutants were obtained, which are 826.45 mg g^{-1} for TC-HCl, 331.01 mg g^{-1} for TC, 1023.88 mg g^{-1} for MO, 726.26 mg g^{-1} for MB, 642.25 mg g^{-1} for DR, respectively. These data are close to the actual adsorption capacity calculated by Eq. (2) (806.37 mg g^{-1} for TC-HCl, 320.56 mg g^{-1} for TC, 1008.56 mg g^{-1} for MO, 706.18 mg g^{-1} for MB, 632.68 mg g^{-1} for DR, respectively). These reported results were significantly higher than those of many reported adsorbents (Table 4).

In order to show the effect of Fe/Cr-codoped on improving ZnO adsorption capacity for the various organic pollutants, the comparison of adsorption capacity on ZnO and Fe/Cr-codoped ZnO for the various organic pollutants were presented in Table 5. It can be seen that the adsorption capacity of Fe/Cr-codoped ZnO is significantly improved compared with that of ZnO.

Based on the above characterization and experimental results, an adsorption mechanism of Fe/Cr-codoped ZnO for the anionic organic pollutants was proposed, as shown

Table 3 Fitting parameters of Langmuir and Freundlich adsorption isotherms for pollutants adsorption (25℃, pH=7.0)

Adsorbate	Langmuir			Freundlich		
	q_m	K_L	R^2	1/n	K_F	R^2
TC-HCl	826.45	0.01127	0.97795	0.262	116.92	0.81424
TC	331.01	0.02032	0.99025	0.319	48.23	0.86150
MO	1023.88	0.01189	0.96535	0.278	139.03	0.83545
MB	726.26	0.01253	0.90560	0.241	122.73	0.77182
DR	642.25	0.00942	0.94961	0.261	92.82	0.84721

Table 4 Comparison of the adsorption capacity for the various adsorbents

Adsorbate	Adsorbent	Adsorption capacity ($mg\ g^{-1}$)	Ref.
TC-HCl	MHNTs	34.00	Guan *et al*., 2012
TC-HCl	g-MoS_2	249.45	Zeng *et al*., 2019
TC-HCl	HT-B	123.6	Ma *et al*., 2018
TC-HCl	MWCNT/NH_2-MIL-53(Fe)	368.49	Xiong *et al*., 2018
TC-HCl	Fe/Cr-codoped ZnO NPs	826.45	This work
TC	CuCo/MIL-101	225.17	Jin *et al*., 2019
TC	Diol-based POPs	155.8	Zhang *et al*., 2018
TC	p-BN	322.16	Song *et al*., 2017
TC	Co-doped UiO-66	224.1	Cao *et al*., 2018
TC	Fe/Cr-codoped ZnO NPs	331.01	This work
MO	Hierarchical structured Fe_2O_3	150.7	Kang *et al*., 2018
MO	chitosan/Al_2O_3/magnetic NPs	417	Haque *et al*., 2014
MO	Amino-MIL-101(Al)	188 ± 9	Tanhaeia *et al*., 2015
MO	Fe_3O_4 MNPs	46.7	Mou *et al*., 2017
MO	Fe/Cr-codoped ZnO NPs	1023.88	This work
MB	Fe_3O_4-CS/EDTA	459.9	Chen *et al*., 2019
MB	Magnetic particles precipitated onto wheat husk	100.0	Shah *et al*., 2014
MB	Na-doped g-C_3N_4	360.0	Fronczak *et al*., 2017
MB	Fe_3O_4@PDA/PEI	172.4	Wang *et al*., 2015
MB	Fe/Cr-codoped ZnO NPs	726.26	This work
DR	$NiFe_2O_4$/AC	299.67	Livani *et al*., 2018
DR	α-CDs-EPI	31.5	Pellicer *et al*., 2018
DR	HP-α-CDs-EPI	23.4	Pellicer *et al*., 2018
DR	AS-CTAB	454.9	Kasperiski *et al*., 2018
DR	Fe/Cr-codoped ZnO NPs	642.25	This work

Table 5 Comparison of the adsorption capacity on ZnO and Fe/Cr-codoped ZnO for the various anionic organic pollutants

	Pollutant	MO	TC-HCl	TC	MB	DR
q ($mg\ g^{-1}$)	ZnO	23.75	21.84	19.56	21.37	28.48
	Fe/Cr-codoped ZnO	1023.88	826.45	331.01	726.26	642.25

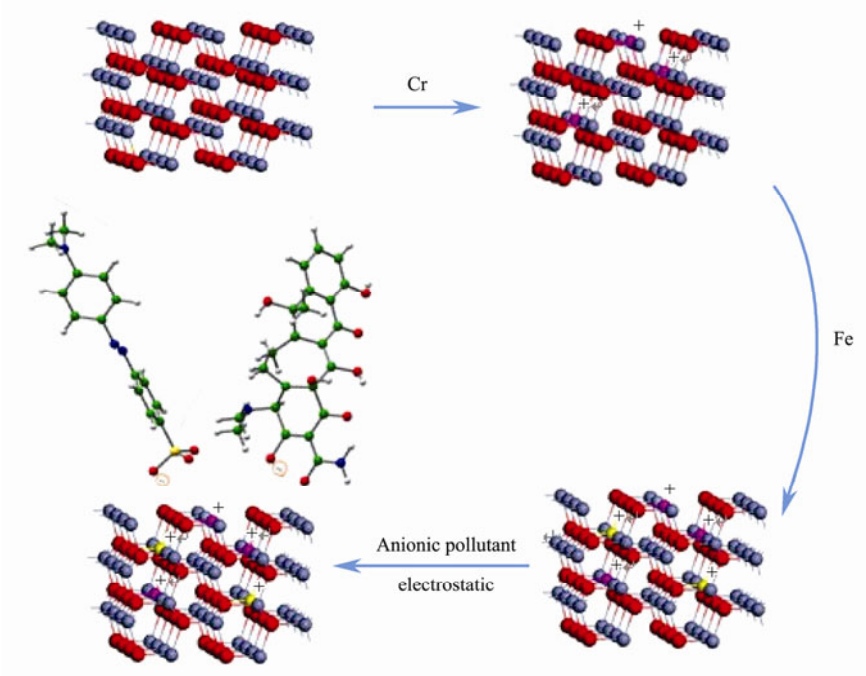

Fig.8 Schematic diagram of the adsorption mechanism of Fe/Cr-codoped ZnO NPs for anionic organic pollutant.

in Fig.8. When Cr^{3+} enters into ZnO lattice to replace Zn^{2+}, the surface of Cr-doped ZnO will have positive charges. However, our previous study showed that when excessive Cr^{3+} was added, a secondary phase ($ZnCrO_4$) would be formed, leading the adsorption capacity decreased. So there is a limit on the doped amount of Cr^{3+}. Therefore, the second metal ionic Fe^{3+} was selected as the dopant to doped ZnO. On the basis of Cr^{3+} doping, some

Fe^{3+} entered into the lattice instead of Zn^{2+} (as shown in XPS), making the surface of Fe/Cr-codoped ZnO have more positive charges, and there's no secondary phase (as shown in XRD) after adding a moderate amount of Fe^{3+}. More positive charge on the surface of dopant would increase the adsorption capacity of the adsorbent for anionic organic pollutant.

The above analysis was confirmed by the results of pH and Zeta potential affecting on the adsorption capacity. It can be seen from the Zeta potential characterization that the surface of Fe/Cr-codoped ZnO has positive charge when pH is within the range of 6–11 in Fig.4. Besides, according to the effect of pH on the adsorption capacity of five pollutants, the more positive charge on the surface of the absorbent, the greater the adsorption capacity is (For example, when pH = 7, Zeta potential is the highest, and the adsorption capacity is also the largest.), indicating that electrostatic interaction is the main adsorption approach. In Fig.8, MO is the representative of three dyes, and TC is the representative of two antibiotics in this work. So, based on the above analysis, Fe/Cr-codoped ZnO NPs can efficient remove anionic organic pollutant by electrostatic interaction.

3.5 Desorption of Pollutant

In practical application, it is very importance for adsorbent to be simple, efficient and non-polluting desorbed and regenerated. In this paper, the separation of adsorbent and pollutant was realized by acid dissolution, alkali precipitation, and finally calcining. Because Fe/Cr-codoped ZnO is soluble in strong acid, it can be dissolved by adding HNO_3, and iron, chromium and zinc will exist in the solution as the ions. When the appropriate amount of NaOH is added to the above solution, the Zn^{2+}, Fe^{3+}, and Cr^{3+} will form hydroxide precipitation. As we all know, the $Ksp(Zn(OH)_2) = 1.2\times10^{-17}$, $Ksp(Cr(OH)_3) = 6.3\times10^{-31}$, and $Ksp(Fe(OH)_3) = 4\times10^{-38}$, so when the pH reaches 8, the Zn^{2+}, Fe^{3+}, and Cr^{3+} in the solution can be completely precipitated. Then, the adsorbent is separated from the contaminant by centrifugation. Finally, the hydroxide precipitates are calcined to obtain their corresponding oxides. The product was characterized by XRD (shown in Fig.9), and it was proved to be ZnO. There is no peak of iron and chromium, which may due to low levels of iron and chromium.

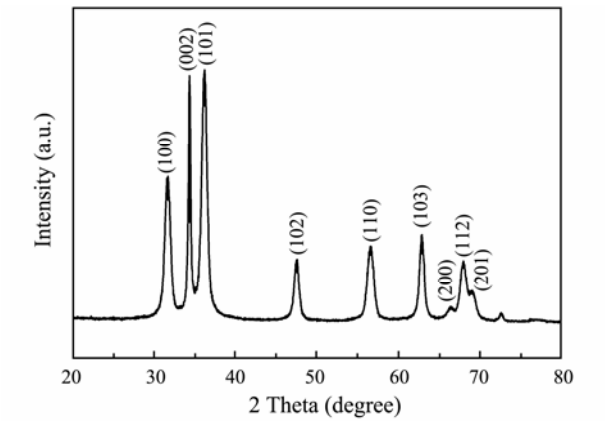

Fig.9 The XRD pattern of the product obtained after the process desorption.

This strategy is as follows:

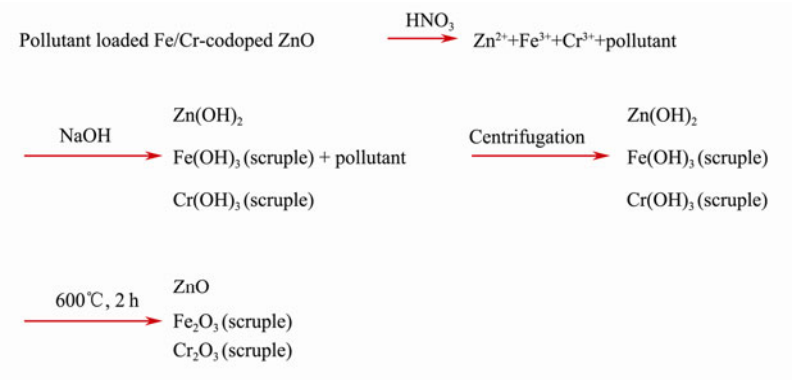

The as-obtained ZnO can be used in other industrial production or synthesis, and the separated pollutants can also be used in industry. Therefore, the whole process will not produce secondary pollution. This kind of adsorbent, which has excellent adsorption performance for anionic organic pollutant and can be reused through simple processing, will become one of the indispensable adsorbents.

4 Conclusions

In summary, nano-sized Fe/Cr-codoped ZnO particles with excellent adsorption performance for the various anionic organic pollutants have been successfully synthesized. The surface of Fe/Cr-codoped ZnO has a large amount of positive charges, which makes it has excellent adsorption performance to the anionic pollutants. The adsorption capacities of the as-prepared adsorbent are up to 826.45, 331.01 mg g^{-1} for the antibiotics of TC-HCl and TC, and 1023.88, 726.26 and 642.25 mg g^{-1} for anionic dyes of MO, MB and DR, respectively. The adsorption of various anionic organic pollutants on Fe/Cr-codoped ZnO NPs was fast, it only took 30 min to reach more than 90% of the equilibrium adsorption amount for TC-HCl, MO, MB and DR, and for TC, it can exceed 90% of its equilibrium adsorption capacity within 10 min. The results of the kinetics study showed that the adsorption of the various anionic organic pollutants followed pseudo-second-order model, and the adsorption process

agreed well to Langmuir isotherm. Most importantly, the desorption of pollutant from the surface of adsorbent was realized by a simple and economic methods. From the above, Fe/Cr-codoped ZnO is an adsorbent with extensive application potential in the field of efficient wastewater treatment.

Acknowledgements

The work was supported by the National Natural Science Foundation of China (Nos. 51672144, 51572137, 51702181), the Natural Science Foundation of Shandong Province (Nos. ZR2017BB013, ZR2019BEM 042), the Higher Educational Science and Technology Program of Shandong Province (Nos. J17KA014, J18KA 001, J18KA033), the Taishan Scholars Program of Shandong Province (No. ts201511034) and the Overseas Taishan Scholars Program. We express our grateful thanks to them for their financial support.

References

Cao, J., Yang, Z. H., Xiong, W. P., Zhou, Y. Y., Peng, Y. R., Li, X., Zhou, C. Y., Xu, R., and Zhang, Y. R., 2018. One-step synthesis of Co-doped UiO-66 nanoparticle with enhanced removal efficiency of tetracycline: Simultaneous adsorption and photocatalysis. *Chemical Engineering Journal*, **353**: 126-137.

Chen, B., Zhao, H. N., Chen, S. J., Long, F. X., Huang, B., Yang, B. Q., and Pan, X. J., 2019. A magnetically recyclable chitosan composite adsorbent functionalized with EDTA for simultaneous capture of anionic dye and heavy metals in complex wastewater. *Chemical Engineering Journal*, **356**: 69-80.

Chen, D. Z., Shen, W. S., Wu, S. L., Chen, C. Q., Luo, X. B., and Guo, L., 2016. Ion exchange induced removal of Pb(II) by MOF-derived magnetic inorganic sorbents. *Nanoscale*, **8**: 7172-7179.

Chen, L., Chen, N. N., Wu, H. M., Li, W. X., Fang, Z., Xu, Z. W., and Qian, X. M., 2018. Flexible design of carbon nanotubes grown on carbon nanofibers by PECVD for enhanced Cr(VI) adsorption capacity. *Separation and Purification Technology*, **207**: 406-415.

Chen, X. L., Cao, Y. G., Lan, Y. C., Xu, X. P., Li, J. Q., Lu, K. Q., Jiang, P. Z., Xu, T., Bai, Z. G., Yu, Y. D., and Liang, J. K., 2000. Synthesis and structure of nanocrystal-assembled bulk GaN. *Journal of Crystal Growth*, **209**: 208-212.

Fronczak, M., Krajewska, M., Demby, K., and Bystrzejewski, M., 2017. Extraordinary adsorption of methyl blue onto sodium-doped graphitic carbon nitride. *The Journal Physical Chemistry C*, **121**: 15756-15766.

Gan, Q. Y., Shi, W. L., Xing, Y. J., and Hou, Y., 2018. A polyoxoniobate/g-C_3N_4 nanoporous material with high adsorption capacity of methylene blue from aqueous solution. *Frontiers in Chemistry*, **6**: 7, https://doi.org/10.3389/fchem.2018.00007.

Ge, X., Song, X. Y., Ma, Y., Zhou, H. J., Wang, G. Z., Zhang, H. M., Zhang, Y. X., Zhao, H. J., and Wong, P. K., 2016. Fabrication of hierarchical iron-containing MnO_2 hollow microspheres assembled by thickness-tunable nanosheets for efficient phosphate removal. *Journal of Materials Chemistry A*, **4**: 14814-14826.

Grosvenor, A. P., Kobe, B. A., Biesinger, M. C., and Mclntyre, N. S., 2004. Investigation of multiplet splitting of Fe 2p XPS spectra and bonding in iron compounds. *Science and Interface Analysis*, **36**: 1564-1574.

Haque, E., Lo, V., Minett, A. I., Harris, A. T., and Church, T. L., 2014. Dichotomous adsorption behaviour of dyes on an amino-functionalised metal-organic framework, amino-MIL-101 (Al). *Journal of Materials Chemistry A*, **2**: 193-203.

Hsu, C. L., Lin, Y. H., Wang, L. K., Hsueh, T. J., Chang, S. P., and Chang, S. J., 2017. Tunable UV- and visible-light photoresponse based on p-ZnO nanostructures/n-ZnO/glass peppered with Au nanoparticles. *ACS Applied Materials and Interfaces*, **9** (17): 14935-14944.

Huang, J. N., Li, Y. H., Cao, Y. H., Peng, F., Cao, Y. G., Shao, Q., Liu, H., and Guo, Z. H., 2018. Hexavalent chromium removal over magnetic carbon nanoadsorbents: Synergistic effect of fluorine and nitrogen co-doping. *Journal of Materials Chemistry A*, **6**: 13062-13074.

Huang, R. Y., Wu, M. J., Zhang, T., Li, D. Q., Tang, P. G., and Feng, Y. J., 2017. Template-free synthesis of large-pore-size porous magnesium silicate hierarchical nanostructures for high-efficiency removal of heavy metal ions. *ACS Sustainable Chemistry and Engineering*, **5**: 2774-2780.

Hu, X. S., Liang, R., and Sun, G. X., 2018. Super-adsorbent hydrogel for removal of methylene blue dye from aqueous solution. *Journal of Materials Chemistry A*, **6**: 17612-17624.

Izaki, M., Chizaki, R., Saito, T., Murata, K., and Shinagawa, T., 2013. Hybrid ZnO/phthalocyanine photovoltaic device with highly resistive ZnO intermediate layer. *ACS Applied Materials and Interfaces*, **5** (19): 9386-9395.

Jin, J. H., Yang, Z. H., Xiong, W. P., Zhou, Y. Y., Xu, R., Zhang, Y. R., Cao, J., Li, X., and Zhou, C. Y., 2019. Cu and Co nanoparticles co-doped MIL-101 as a novel adsorbent for efficient removal of tetracycline from aqueous solutions. *Science of the Total Environment*, **650**: 408-418.

Kang, D. J., Hu, C. Q., and Zhu, Q. S., 2018. Morphology controlled synthesis of hierarchical structured Fe_2O_3 from natural ilmenite and its high performance for dyes adsorption. *Applied Surface Science*, **459**: 327-335.

Kasperiski, F. M., Lima, E. C., Reis, G. S. D., Costa, J. B. D., Dotto, G. L., Dias, S. L. P., Cunha, M. R., Pavan, F. A., and Correa, C. S., 2018. Preparation of CTAB-functionalized aqai stalk and its efficient application as adsorbent for the removal of Direct Blue 15 and Direct Red 23 dyes from aqueous media. *Chemical Engineering Commununications*, **205**: 1520-1536.

Li, C. R., Zhuang, Z. Y., Huang, F., Wu, Z. C., Hong, Y. P., and Lin, Z., 2013. Recycling rare earth elements from industrial wastewater with flowerlike nano-$Mg(OH)_2$. *ACS Applied Materials and Interfaces*, **5**: 9719-9725.

Li, H., Bao, H. Q., Song, B., Wang, W. J., and Chen, X. L., 2008. Observation of ferromagnetic ordering in Ni-doped AlN polycrystalline powders. *Solid State Communications*, **148**: 406-409.

Li, M. R., Wei, D., Liu, T., Liu, Y. R., Yan, L. G., Wei, Q., Du, B., and Xu, W. Y., 2019. EDTA functionalized magnetic biochar for Pb(II) removal: Adsorption performance, mechanism and SVM model prediction. *Separation and Purification Technology*, **227**: 115696.

Li, S. J., Chen, J. L., Hu, S. W., Jiang, W., Liu, Y. P., and Liu, J. S., 2020. A novel 3D Z-scheme heterojunction photocatalyst: $Ag_6Si_2O_7$ anchored on flower-like Bi_2WO_6 and its excellent photocatalytic performance for the degradation of toxic pharmaceutical antibiotics. *Inorganic Chemistry Frontiers*, **7**: 529-541.

Li, T., Ma, S., Yang, H., and Xu, Z. L., 2019. Preparation of carbonized MOF/$MgCl_2$ hybrid products as dye adsorbent and supercapacitor: Morphology evolution and Mg salt effect. *Industrial and Engineering Chemistry Research*, **58** (4): 1601-1602, DOI: 10. 1021/acs.iecr.8b06437.

Li, X., Liu, S. W., Fan, K., Liu, Z. Q., Song, B., and Yu, J. G., 2018. MOF-based transparent passivation layer modified ZnO nanorod arrays for enhanced photoelectrochemical water splitting. *Advanced Energy Materials*, **8**: 1800101.

Li, Z. J., Sun, Y. K., Xing, J., Xing, Y. C., and Meng, A. L., 2018. One step synthesis of Co/Cr-codoped ZnO nanoparticle with superb adsorption properties for various anionic organic pollutants and its regeneration. *Journal of Hazardous Materials*, **352**: 204-214.

Li, Z. J., Xing, Y. C., Fan, X. Y., Lin, L. G., Meng, A. L., and Li, Q. D., 2018. rGO/protonated gC_3N_4 hybrid membranes fabricated by photocatalytic reduction for the enhanced water desalination. *Desalination*, **443**: 130-136.

Livani, M. J., and Ghorbani, M., 2018. Fabrication of $NiFe_2O_4$ magnetic nanoparticles loaded on activated carbon as novel nanoadsorbent for Direct Red 31 and Direct Blue 78 adsorption. *Environmental Technology*, **39**: 2977-2993.

Lo, K., and Irene, M., 2017. Removal of ionizable aromatic pollutants from contaminated water using nano γ-Fe_2O_3 based magnetic cationic hydrogel: Sorptive performance, magnetic separation and reusability. *Journal of Hazardous Materials*, **322**: 195- 204.

Ma, C. C., Huang, H., Gao, X., Wang, T., Zhu, Z., Huo, P. W., Liu, Y., and Yan, Y. S., 2018. Honeycomb tubular biochar from fargesia leaves as an effective adsorbent for tetracyclines pollutants. *Journal of the Taiwan Institute of Chemical Engineers*, **91**: 299-308.

Musielak, M., Gagor, A., Zawisza, B., Talik, E., and Sitko, R., 2019. Graphene oxide/carbon nanotube membranes for highly efficient removal of metal ions from water. *ACS Applied Materials and Interfaces*, **11**: 28582-28590.

Okesola, B., and Smith, D., 2016. Applying low-molecular weight supramolecular gelators in an environmental setting-self-assembled gels as smart materials for pollutant removal. *Chemical Society Reviews*, **45**: 4226-4251.

Pellicer, J. A., Rodríguez-López, M. I., Fortea, M. I., Hernandez, J. A. G., Lucas-Abellan, C., Mercader-Ros, M. T., Serrano-Martinez, A., Nunez-Delicado, E., Cosma, P., Fini, P., Franco, E., Garcia, R., Ferrandiz, M., Perez, E., and Ferrandiz, M., 2018. Removing of direct red 83:1 using α-and HP-α-CDs polymerized with epichlorohydrin: Kinetic and equilibrium studies. *Dyes and Pigments*, **149**: 736-746.

Peng, Q. M., Guo, J. X., Zhang, Q. R., Xiang, J. Y., Liu, B. Z., Zhou, A. G., Liu, R. P., and Tian, Y. J., 2014. Unique lead adsorption behavior of activated hydroxyl group in two-dimensional titanium carbide. *Journal of American Chemical Society*, **136**: 4113-4116.

Perreault, F., Fonseca de Faria, A., and Elimelech, M., 2015. Environmental applications of graphene-based nanomaterials. *Chemical Society Reviews*, **44**: 5861-5896.

Qi, C. Y., Zhao, L. Q., Lin, Y., and Wu, D. Y., 2018. Graphene oxide/chitosan sponge as a novel filtering material for the removal of dye from water. *Journal of Colloid and Interface Science*, **517**: 18-27.

Rekha, P., Muhammad, R., Sharma, V., Ramteke, M., and Mohanty, P., 2016. Unprecedented adsorptive removal of $Cr_2O_7^{2-}$ and methyl orange by using a low surface area organosilica. *Journal of Materials Chemistry A*, **4**: 17866-17874.

Roosen, J., and Binnemans, K., 2014. Adsorption and chromatographic separation of rare earths with EDTA- and DTPA-functionalized chitosan biopolymers. *Journal of Materials Chemistry A*, **2**: 1530-1540.

Shah, J., Jan, M. R., Jamil, S., and Haq, A. U., 2014. Magnetic particles precipitated onto wheat husk for removal of methyl blue from aqueous solution. *Toxicological Environmental Chemistry*, **96**: 218-226.

Shen, X. C., Ma, S., Xia, H., Shi, Z., Mu, Y., and Liu, X. M., 2018. Cationic porous organic polymers as an excellent platform for highly efficient removal of pollutants from water. *Journal of Materials Chemistry A*, **6**: 20653-20658.

Song, B., Chen, X. L., Han, J. C., Wang, G., Bao, H. Q., Zhu, K. X., Li, H., Zhang, Z. H., Wang, W. Y., Wang, W. J., Zhang, X. H., and Meng, S. H., 2011. Raman scattering and magnetizations studies of (Al, Cr)-codoped 4H-SiC. *Journal of Magnetism and Magnetic Materials*, **323**: 2876-2882.

Song, Q. Q., Fang, Y., Liu, Z. Y., Li, L. L., Wang, Y. R., Liang, J. L., Huang, Y., Lin, J., Hu, L., Zhang, J., and Tang, C. C., 2017. The performance of porous hexagonal BN in high adsorption capacity towards antibiotics pollutants from aqueous solution. *Chemical Engineering Journal*, **325**: 71-79.

Song, Y. L., Wang, X. J., Zhang, X. Q., Qi, X. D., Liu, Z. G., Zhang, L. L., Zhang, Y., Wang, Y., Sui, Y., and Song, B., 2016. Colossal dielectric permittivity in (Al + Nb) co-doped rutile SnO_2 ceramics with low loss at room temperature. *Applied Physics Letters*, **109**: 142903.

Tanhaeia, B., Ayatia, A. A., Lahtinenb, M., and Sillanpaa, M., 2015. Preparation and characterization of a novel chitosan/Al_2O_3/magnetite nanoparticles composite adsorbent for kinetic, thermodynamic and isotherm studies of methyl orange adsorption. *Chemical Engineering Journal*, **259**: 1-10.

Wang, X. Y., Cai, J. H., Zhang, Y. J., Li, L. H., Jiang, L., and Wang, C. R., 2015. Heavy metal sorption properties of magnesium titanate mesoporous nanorods. *Journal of Materials Chemistry A*, **3**: 11796-11800.

Wang, Z., Guo, J., Ma, J., and Shao, L., 2015. Highly regenerable alkali-resistant magnetic nanoparticles inspired by mussels for rapid selective dye removal offer high-efficiency environmental remediation. *Journal of Materials Chemistry A*, **3**: 19960-19968.

Wu, Z. X., Li, W., Webley, P. A., and Zhao, D. Y., 2012. General and controllable synthesis of novel mesoporous magnetic iron oxide@carbon encapsulates for efficient arsenic removal. *Advanced Materials*, **24**: 485-491.

Xiong, W. P., Zeng, Z. T., Li, X., Zeng, G. M., Xiao, R., Yang, Z. H., Zhou, Y. Y., Zhang, C., Cheng, M., Hu, L., Zhou, C. Y., Qin, L., Xu, R., and Zhang, Y. R., 2018. Multi-walled carbon nanotube/amino-functionalized MIL-53 (Fe) composites: Remarkable adsorptive removal of antibiotics from aqueous solutions. *Chemosphere*, **210**: 1061-1069.

Yang, J., Zhang, H. W., Yu, M. H., Emmanuelawati, I., Zou, J., Yuan, Z. G., and Yu, C. Z., 2014. High-content, well-dispersed γ-Fe_2O_3 nanoparticles encapsulated in macroporous silica with superior arsenic removal performance. *Advanced Functional Materials*, **24**: 1354-1363.

Yao, L., Zhang, L. Z., Wang, R., Chou, S. R., and Dong, Z. L., 2016. A new integrated approach for dye removal from wastewater by polyoxometalates functionalized membranes. *Journal of Hazardous Materials*, **301**: 462-470.

Yu, X. Y., Xu, R. X., Gao, C., Luo, T., Jia, Y., Liu, J. H., and Huang, X. J., 2012. Novel 3D hierarchical cotton-candy-like CuO: Surfactant-free solvothermal synthesis and application in As(III) removal. *ACS Applied Materials and Interfaces*, **4**: 1954-1962.

Zeng, Z. T., Ye, S. J., Wu, H. P., Xiao, R., Zeng, G. M., Liang, J., Zhang, C., Yu, J. F., Fang, Y. L., and Song, B., 2019. Research on the sustainable efficacy of g-MoS_2 decorated biochar nanocomposites for removing tetracycline hydrochloride from antibiotic-polluted aqueous solution. *Science of the Total Environment*, **648**: 206-217.

Zhang, H., Sun, J. M., Dagle, V. L., Halevi, D., Datye, A. K., and Wang, Y., 2014. Influence of ZnO facets on Pd/ZnO catalysts for methanol steam reforming. *ACS Catalysis*, **4** (7): 2379-2386.

Zhang, L., Wang, J., Ren, X. Y., Zhang, W. T., Zhang, T. S., Liu, X. N., Du, T., and Wang, J. L., 2018. Internally extended growth of core-shell NH_2-MIL-101(Al)@ZIF-8 nanoflowers for the simultaneous detection and removal of Cu(II). *Journal of Materials Chemistry A*, **6**: 21029-21038.

Zhang, S. P., Li, Y. K., Shi, C. H., Guo, F. Y., He, C. Z., Cao, Z., Hu, J., Cui, C. Z., and Liu, H. L., 2018. Induced-fit adsorption of diol-based porous organic polymers for tetracycline remo- val. *Chemosphere*, **212**: 937-945.

Zhao, R., Li, X., Sun, B., Li, Y. Z., Li, Y. M., Yang, R., and Wang, C., 2017. Branched polyethylenimine grafted electrospun polyacrylonitrile fiber membrane: A novel and effective adsorbent for Cr(VI) remediation in wastewater. *Journal of Materials Chemistry A*, **5**: 1133-1144.

Zheng, X. N., Wu, D. B., Su, T., Bao, S., Liao, C. A., and Wang, Q. G., 2014. Magnetic nanocomposite hydrogel prepared by ZnO-initiated photopolymerization for La(III) adsorption. *ACS Applied Materials and Interfaces*, **6**: 19840-19849.

Zhou, L. J., Ying, G. G., Liu, S., Zhang, R. Q., Lai, H. J., Chen, Z. F., and Pan, C. G., 2013. Excretion masses and environmental occurrence of antibiotics in typical swine and dairy cattle farms in China. *Science of the Total Environment*, **444**: 183-195.

Zhu, Y. G., Johnson, T. A., Su, J. Q., Qian, M., Guo, G. X., Stedtfeld, R. D., Hashsham, S. A., and Tiedje, J. M., 2013. Diverse and abundant antibiotic resistance genes in Chinese swine farms. *Proceedings of the National Academy Sciences of the United States of America*, **110**: 3435-3440.

Zou, J., Wu, K., Wu, H. D., Guo, J., and Zhang, L. F., 2020. Synthesis of heterostructure d-MnO_2/h-MoO_3 nanocomposite and the enhanced photodegradation activity of methyl orange in aqueous solutions. *Journal of Material Science*, **55**: 3329-3346.

(Edited by Ji Dechun)